PROCEEDINGS OF SCIENCE

Detection of Cosmic Rays at High Elevation by the BEACON Prototype

Andrew Zeolla[a,b,*] **and Zachary Martin**[c] **for the BEACON Collaboration**
(a complete list of authors can be found at the end of the proceedings)

[a] *Department of Physics, Pennsylvania State University, University Park, PA 16802, USA*
[b] *Center for Multimessenger Astrophysics, Institute of Gravitation and the Cosmos, Pennsylvania State University, University Park, PA 16802, USA*
[c] *Department of Physics, Kavli Institute for Cosmological Physics, University of Chicago, Chicago, IL 60637, USA*

E-mail: azeolla@psu.edu

The Beamforming Elevated Array for COsmic Neutrinos (BEACON) is a detector concept designed to measure the flux of Earth-skimming tau neutrinos above 100 PeV. BEACON will consist of many independent, phased radio arrays placed on mountains. The long in-air propagation length of radio together with the high-elevation sites provide BEACON with a large detector volume in an efficient manner. A prototype, consisting of a single phased array, is located in the White Mountains of California. In 2021, the phased array consisted of four cross-polarized short-dipole antennas. In 2023, the original antennas were replaced with six newly designed antennas, deployed alongside an independent array of four scintillators. The goal of the prototype is to demonstrate its ability to trigger on the radio emission of extensive air showers by first detecting cosmic rays. Here, we present cosmic ray candidates from two independent cosmic ray searches: a radio-triggered search using data from the 2021 instrument, and a scintillator-triggered search for coincident radio signal using data from the 2023 instrument. In the future, this measurement of the cosmic ray flux will be used to perform an in-situ validation of BEACON's predicted energy threshold.

39th International Cosmic Ray Conference (ICRC2025)
15–24 July 2025
Geneva, Switzerland

ICRC 2025
The Astroparticle Physics Conference
Geneva July 15-24, 2025

*Speaker

PoS(ICRC2025)444

1. Introduction

The Beamforming Elevated Array for COsmic Neutrinos (BEACON) is a proposed neutrino detector, designed to measure the flux of tau neutrinos above 100 PeV [1]. Ultrahigh energy tau neutrinos which skim the Earth can interact within, producing a tau lepton which can then escape the Earth and decay in the atmosphere, creating an up-going extensive air shower (EAS) [2]. BEACON targets the geomagnetic radio emission of these up-going EAS, using $O(1000)$ digitally-phased radio antenna arrays placed on mountains. The high-elevation sites provide BEACON with a very large instantaneous effective area, while beamforming reduces the energy threshold and thus enhances the sensitivity.

The BEACON prototype consists of a single phased array located in the White Mountains of California [3]. It has been operating in various iterations since 2018. One of the primary goals of the BEACON prototype is to demonstrate the capability of detecting geomagnetic radio emission using a phased array at high altitude. A single array is unlikely to detect an ultrahigh energy tau neutrino however, so instead the prototype targets down-going EAS initiated by cosmic rays. The cosmic ray flux at high energies is significantly greater and well-constrained [4]. We can thus estimate the energy threshold of the BEACON prototype by comparing its measurement of the cosmic ray flux to existing measurements.

Here, we detail the analysis and results of two independent cosmic ray searches performed for the BEACON prototype: an on-going "radio-only" search using the phased array trigger from the 2021 prototype, and a "radio and scintillator coincidence" search using scintillator-triggered data from the 2023 prototype.

2. Radio-Only Cosmic Ray Search

2.1 The 2021 BEACON Prototype

The 2021 prototype consisted of four crossed-dipole antennas for a total of 8 channels. The four antennas were located on the eastern slope of Mt. Barcroft, in the White Mountains of California, at an altitude of 3.8 km above sea level. The four horizontally-polarized channels were digitally-phased to form the trigger. In digital beamforming, the signals received by each antenna are delayed and summed according to a table of pre-programmed time delays coinciding with different arrival directions, or beams. If a radio source is located within one of these beams, then delaying the signals will align them. Summing the signals will thus lead to a greater signal-to-noise ratio (SNR). A digitally-phased array therefore has a greater sensitivity than an array of independent antennas. The design of the 2021 prototype is described in detail in [3].

Here, we present the analysis of events recorded from August 27 to December 18, 2021. This corresponds to the time period between the 2021 deployment and a winter storm which damaged one of the channels. Across the $\sim$ 113 days of data, $\sim$ 100 million events were recorded. Of the $\sim$ 1 million events per day, fewer than 1 are expected to be a cosmic ray. Achieving a low background estimate is therefore imperative.

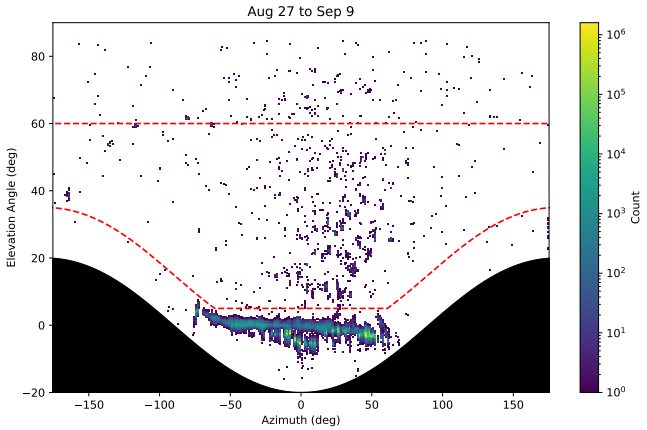

Figure 1: The reconstructed arrival direction for events recorded from August 27 to September 9, 2021, which pass quality cuts. We restrict the cosmic ray search to the region depicted in red.

2.2 Analysis

The direction of the source of each event is first determined. This is done by creating a correlation map, essentially a map of how well the waveforms align given the time delays predicted by each direction in space. For an impulsive event like a cosmic ray, there will be one very bright spot on the map corresponding to the direction of the source, followed by a few less bright spots corresponding to directions which produce partial waveform alignment. These directions are referred to as the mainlobe and sidelobes, respectively. The peak-to-sidelobe ratio is the ratio between the correlation value at the mainlobe to the correlation value at the brightest sidelobe. Correlation maps are generated for both polarizations for a given event, and the map with the higher peak-to-sidelobe ratio is selected. Another measurement of reconstruction accuracy is the correlation ratio. The correlation value at the mainlobe is compared to the theoretical maximum correlation value that could be produced between all the waveforms.

All events are first filtered. This includes a digital bandpass from 30-80 MHz, a digital bandstop from 52.5-60.5 MHz, and sine-subtraction. As a quality cut, events with correlation ratios below 0.9 are removed. Additionally, events with signal-to-noise ratios of NaN, inf, or zero are removed (typically caused by a glitched readout). Lastly, events with signals which occur very early or very late in the readout window are removed. Overall, these quality cuts remove only $\sim 0.5\%$ of events. A subset of the remaining events (12.5 days) are shown in Fig. 1. The below-horizon events are mostly anthropogenic in origin, with many clustering on known sources [3]. We therefore restrict our search to the region depicted in red. Only 0.071% of events occur within this region.

The cosmic ray search for the remaining events has two branches: a series of cuts to determine if an event is "cosmic-ray-like", and a temporospatial clustering cut to determine if an event is isolated in both time and space. A cosmic ray event should be both cosmic-ray-like and isolated. The amount of background events which leak into the signal region can then be estimated using the proportion of events which pass each arm of the search (the ABCD method [5]).

The first of the cosmic-ray-like cuts is a Linear Discriminant Analysis (LDA), trained on

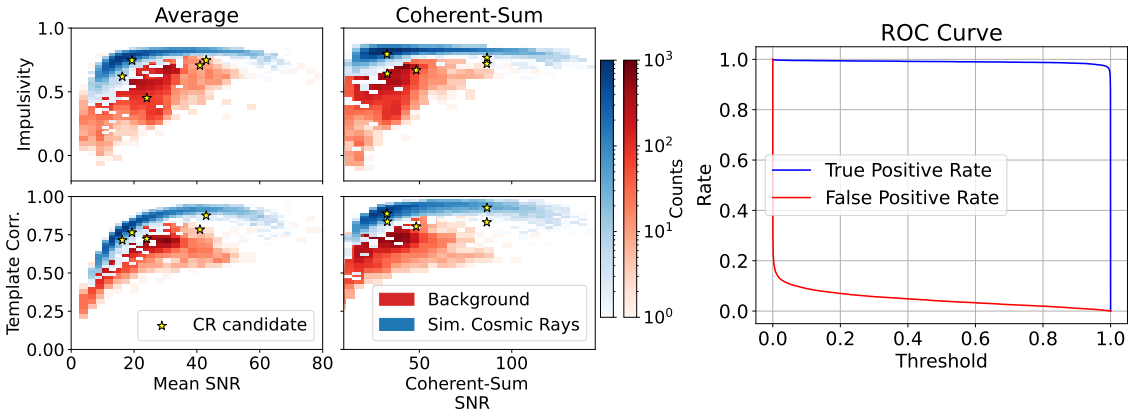

Figure 2: Left: 2-D histograms of impulsivity and template correlation versus signal-to-noise ratio for the horizontally-polarized channels. On the left are values averaged across the four channels of an event, and on the right are values from their coherent-sum. The distributions for simulated cosmic rays (blue) are overlaid on the distributions for background events (red). Also shown are the values obtained for the five cosmic ray candidates (yellow stars). Right: The resulting ROC curve after LDA training.

simulated cosmic ray events and real background. The background events are sampled from events outside the search region. The simulated cosmic rays come from the cosmic ray Monte Carlo for BEACON, CRANBERRY [6]. CRANBERRY fully simulates cosmic ray signals by convolving electric fields from ZHAireS [7] with the simulated prototype antenna model and the measured prototype signal-chain. These simulated signals are then added to real noise traces to create simulated events. Additionally, the signals can be used to create a cosmic ray template. Simulated cosmic rays are sampled based on the energy distribution predicted by CRANBERRY and the cosmic ray flux measured by Auger [4].

2-D histograms of the horizontally-polarized impulsivity (see [3] for definition) and template correlation versus signal-to-noise ratio (SNR) are shown on the left in Fig. 2. The impulsivity and template correlation are calculated for each of the channels of an event, and the average per polarization is calculated. The values for the coherently-summed waveforms are also calculated. The LDA is trained to separate cosmic rays from background using these distributions and those of the vertically-polarized channels. The resulting ROC curve, depicting the LDA's classification accuracy, is shown on the right in Fig. 2.

The polarization of geomagnetic emission is determined by $\vec{v} \times \vec{B}$, where $\vec{v}$ is the cosmic ray propagation vector, and $\vec{B}$ is the local geomagnetic field. The measured polarization is then further determined by the prototype antenna model. Using Stokes parameters Q and U, the polarization angle is defined as $\theta_p = 0.5 \arctan(U/Q)$. A fully-horizontal signal has $\theta_p = 0°$, while a fully-vertical signal has $\theta_p = 90°$. Overall, 96.6% of simulated cosmic rays have θ_p greater than 10° and less than 45°. Additionally, 99.6% of simulated cosmic rays have linear polarization factors greater than 0.75. These thresholds have been implemented as additional cosmic-ray-like cuts. Overall, with these cuts and an LDA threshold of 0.9, only 0.11% of events in the search region are determined to be cosmic-ray-like.

For the temporospatial cut, the angular distance between event i and event j has been defined

as

$$d = \sqrt{\left[(\theta_i - \theta_j)^2 + (\phi_i - \phi_j)^2\right]}. \quad (1)$$

Events which occur within 10 minutes of each other, and have $d \leq 20°$, are determined to be clustered. The primary intent of this cut is to remove transient above-horizon anthropogenic events, like airplanes, which can mimic cosmic rays but occur in bursts. Overall, only 9.6% of analyzed events are isolated.

2.3 Results

Mis-reconstructed events, as well as strange events likely caused by amplifier instability, can lead to seemingly isolated events which pass cosmic-ray-like cuts. Additional quality cuts are therefore being developed to identify and remove these events. For now, we have identified five preliminary cosmic ray candidates, shown in Fig. 3. One of these candidates was independently identified as a potential cosmic ray in our previous impulsive event search [3]. Three others occur behind the array. Given the high SNR of these events, it is unsurprising that they still manage to trigger the phased array despite being outside of the beam pattern. Their presence, however, suggests that there should be many more similar events detected within the beam pattern. We are currently investigating this discrepancy.

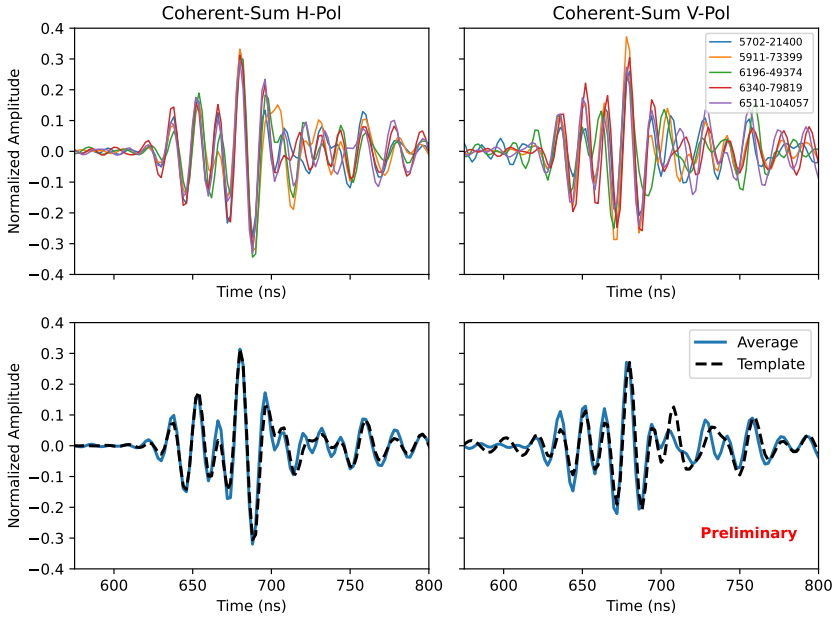

Figure 3: The coherently-summed, filtered waveforms of the 5 cosmic ray candidate events. On the left is the horizontal-polarization, and on the right is the vertical-polarization. Below is the average of the 5 sums compared to the cosmic ray template produced using CRANBERRY.

3. Radio and Scintillator Coincidence Search

3.1 The 2023 BEACON Prototype

In 2023, the existing antennas were replaced with an improved crossed-dipole design. The new design featured a non-conductive fiberglass mast, improved shielding, and stronger antenna tines. The size of the array was also increased to 6 antennas, for a total of 12 radio channels, which also necessitated an upgraded DAQ. A scintillator array consisting of four IceTop scintillators [8] was embedded among the radio array, to serve as a independent detector for cosmic ray events via the detection of secondary muons.

A new coincidence trigger was developed such that when three out of four scintillators record a signal above threshold, both scintillator and radio data are saved. By studying events which are confirmed to be cosmic rays by the scintillators, we can make improvements to the phased-array trigger design. Additionally, scintillators generally have a lower energy threshold, allowing us to study events which the radio array would have likely failed to record.

3.2 Analysis

The dataset covers BEACON up-time from October 19, 2023 to March 2, 2024 and consists of nearly 25 million events. We build seven cuts motivated by quality control, expected RF (radio-frequency) behavior, and metrics to determine RF-scintillator coincidence. These cuts are summarized in Table 1.

A positive correlation was found between high winds and event rate. This is likely vibration on electronics or storms with lightning, and thus we remove events with winds greater than 8mph according to the Dendra database for White Mountain, Barcroft Station.

RF cuts are performed using the horizontally-polarized channels, where the cosmic ray radio signal is expected to be strongest. The cuts use the peak of the Hilbert envelope, SNR, impulsivity, and zenith as metrics for expected RF behavior. The Hilbert envelope peak cut removes impulses that are cut-off at the beginning or end of the recorded waveform. The reconstructed direction in RF is obtained similarly to that in the 2021 cosmic ray analysis discussed earlier, using correlation maps. Events in which the RF reconstructs below the horizontal are removed.

Impulsive background events and their mis-reconstructions tend to cluster. These clusters are identified by DBSCAN clustering on force-triggered events which possess RF-impulsive traits (determined by the RF cuts above). This cluster map is Gaussian blurred (with an increasing deviation in azimuth as zenith decreases to accurately represent the changing area on the spatial grid) and normalized to give a "probability-like" value where a value of 1 suggests the point is in a RF noise cluster, and 0 suggests the point is not in a RF noise cluster.

A final cut is made on the angular distance between the reconstructed direction from RF, and the reconstructed direction from the scintillators. The reconstruction with the scintillator array is calculated using arrival time differences of scintillator pulses with respect to one another. Then we minimize the loss function at each azimuth and zenith bin,

$$\chi(\theta,\phi)^2 = \sum_{ij} \frac{(\Delta t_{\mathrm{meas},ij}(\theta,\phi) - \Delta t_{\mathrm{exp},ij}(\theta,\phi))^2}{\delta(\Delta t_{\mathrm{meas},ij}(\theta,\phi))^2}$$

	Cut Name	Restriction	Remaining Events	Cut % (Sequential)	Cut % (as first)
0	Full	None	25,209,347	0.00%	0.00%
1	RF H Zenith	$x < 90°$	11,549,103	54.19%	28.12%
2	RF H Hilb. Peak	$0.01 > x > 0.9$	9,355,980	18.99%	4.51%
3	RF H Impulsivity	$x > 0.6$	36,768	99.61%	19.19%
4	RF H SNR	$5 > x > 25$	29,592	19.52%	0.01%
5	Wind Speed	$x < 8$mph	25,691	13.18%	0.01%
6	RF Noise-Like	$x < 0.01$	1,310	94.90%	0.05%
7	RF-Scint Distance	$x < 10$	15	98.85%	0.002%

Table 1: The cuts used in the 2023 RF-scintillator analysis.

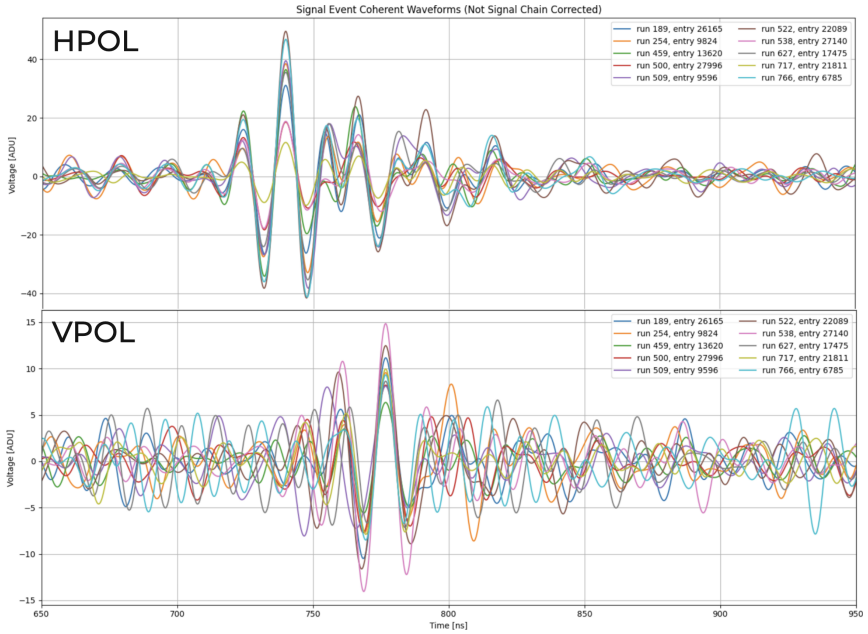

Figure 4: The unfiltered RF waveforms of the 10 cosmic ray candidate events from the 2023 RF-scintillator coincidence search. Note that the V-pol waveforms were coherently summed using the timing delays determined by H-pol waveforms.

where the expected time differences $\Delta t_{\text{exp},ij}$ are obtained using calibrated detector positions and plane wave assumption.

3.3 Results

After applying these cuts, we are left with 15 events that have coincident RF and scintillator signals. We estimate the number of background events which may leak into the signal region by randomly pairing force-triggered RF data with scintillator-triggered scintillator data. In this synthetic dataset, we guarantee that no RF is associated with the scintillator, and thus they should not pass all cuts discussed, except by chance. We perform this on different randomization seeds in order to collect background statistics. We obtain a background of 8 ± 1 events.

We note that 10 of the 15 candidate events have saturated scintillator signals. It is likely that cosmic ray radio signals that can be seen by BEACON are produced by such highly energetic cosmic rays that the scintillator digitizer becomes saturated. Simulations which model both the radio emission with CRANBERRY and the scintillator signal with GEANT4 are currently being developed to test this. Nonetheless, saturated scintillators may be an indicator of cosmic rays with significant radio emission. Among all scintillator data, only 6.8% of events are saturated. Thus by applying another cut which removes non-saturated scintillator signals, we are left with 10 events on an estimated background of only 1. The coherently-summed RF waveforms of these 10 events are shown in Figure 4.

4. Conclusions

Two independent cosmic ray searches are being conducted for the BEACON prototype. These searches together can be used to verify the predicted performance of a BEACON-like detector. The first, using events collected by the phased radio array of 2021, has identified 5 cosmic ray candidates. These candidates correlate well with the cosmic ray template produced by CRANBERRY. Interestingly, three of the five candidates occur behind the array, suggesting that there may be "missing" candidates in the forward direction. We are currently investigating potential causes of this, such as an imperfect calibration. Once the cuts are finalized, a background estimate will be performed using the ABCD method. Validation will be performed using the predicted polarization angle and airplane location data.

The second search utilizes a scintillator array installed in 2023. A scintillator trigger, in coincidence with cosmic-ray-like impulses, serves as validation of cosmic ray detection. This search has identified 15 events which have radio impulses coincident with scintillator signals, on an expected background of 8 ± 1 events. If we assume that scintillator saturation is evidence of a high-energy cosmic ray, and add an additional cut based on this, then we are left with 10 events on an expected background of 1. We are currently developing a Monte Carlo to test this assumption.

References

[1] S. Wissel et al., *Prospects for high-elevation radio detection of >100 PeV tau neutrinos*, *JCAP* **11** (2020) 065 [2004.12718].

[2] E. Zas, *Neutrino detection with inclined air showers*, *New Journal of Physics* **7** (2005) 130.

[3] D. Southall et al., *Design and Initial Performance of the Prototype for the BEACON Instrument for Detection of Ultrahigh Energy Particles*, *NIM-A* **1048** (2023) 167889 [2206.09660].

[4] Pierre Auger collaboration, *The energy spectrum of cosmic rays beyond the turn-down around* 10^{17} *eV as measured with the surface detector of the Pierre Auger Observatory*, *Eur. Phys. J. C* **81** (2021) 966 [2109.13400].

[5] G. Kasieczka, B. Nachman, M.D. Schwartz and D. Shih, *Automating the ABCD method with machine learning*, *Phys. Rev. D* **103** (2021) 035021 [2007.14400].

[6] A. Zeolla et al., *The Beamforming Elevated Array for COsmic Neutrinos (BEACON): A Radio Detector for Earth-Skimming Tau Neutrinos*, *PoS* **ARENA2022** (2022) 023.

[7] J. Alvarez-Muñiz, W.R. Carvalho and E. Zas, *Monte Carlo simulations of radio pulses in atmospheric showers using ZHAireS*, *Astroparticle Physics* **35** (2012) 325–341.

[8] T. Huber, J. Kelley, S. Kunwar and D. Tosi, *The IceTop Scintillator Upgrade*, in *Proceedings of 35th International Cosmic Ray Conference — PoS(ICRC2017)*, vol. 301, p. 401, 2017, DOI.

Full Author List: BEACON Collaboration (July 1st, 2025)

J. Alvarez-Muñiz[1], S. Cabana-Freire[1], W. Carvalho Jr.[2], A. Cummings[3,4,5], C. Deaconu[6], J. Hinkel[3], K. Hughes[7], R. Krebs[3,4], Y. Liu[7], Z. Martin[8], K. Mulrey[9,10] A. Nozdrina[7], E. Oberla[6], S. Prohira[11], A. Romero-Wolf[12], A. G. Vieregg[6,8,13], S. A. Wissel[3,4,5], E. Zas[1], A. Zeolla[3,4]

[1]Instituto Galego de Física de Altas Enerxías IGFAE, Univerisade de Santiago de Compostela, 15782 Santiago de Compostela, Spain
[2]Faculty of Physics, University of Warsaw, 02-093, Warsaw, Poland
[3]Department of Physics, Pennsylvania State University, University Park, PA 16802, USA
[4]Center for Multimessenger Astrophysics, Institute of Gravitation and the Cosmos, Pennsylvania State University, University Park, PA 16802, USA
[5]Department of Astronomy and Astrophysics, Pennsylvania State University, University Park, PA 16802, USA
[6]Department of Astronomy and Astrophysics, Kavli Institute for Cosmological Physics, University of Chicago, Chicago, IL 60637, USA
[7],Department of Physics, The Ohio State University, Columbus, OH 43210, USA
[8]Department of Physics, Kavli Institute for Cosmological Physics, University of Chicago, Chicago, IL 60637, USA
[9]Department of Astrophysics / IMAPP, Radboud University Nijmegen, 6500 GL, Nijmegen, The Netherlands
[10]NIKHEF, Science Park Amsterdam, 1098 XG, Amsterdam, The Netherlands
[11]Department of Physics and Astronomy, University of Kansas, Lawrence, KS 66045, USA
[12]Jet Propulsion Laboratory, California Institute for Technology, Pasadena, CA 91109, USA
[13]Enrico Fermi Institute, University of Chicago, Chicago, IL 60637, USA

Acknowledgments

This work is supported by NSF Awards # 2033500, 1752922, 1607555, and DGE-1746045 as well as the Sloan Foundation, the RSCA, the Bill and Linda Frost Fund at the California Polytechnic State University, and NASA (support through JPL and Caltech as well as Award # 80NSSC18K0231). This work has received financial support from Ministerio de Ciencia, Innovación y Universidades/Agencia Estatal de Investigación, MICIU/AEI/10.13039/501100011033, Spain (PID2022-140510NB-I00, PCI2023-145952-2, RYC2019-027017-I, and María de Maeztu grant CEX2023-001318-M); Xunta de Galicia, Spain (CIGUS Network of Research Centers and Consolidación 2021 GRC GI-2033 ED431C-2021/22 and 2022 ED431F-2022/15); and Feder Funds. We thank the NSF-funded White Mountain Research Station for their support. Computing resources were provided by the University of Chicago Research Computing Center and the Institute for Computational and Data Sciences at Penn State.

PoS(ICRC2025)444